



Computational Analysis for Good Thermal Exchange and Low Pressure Drop in Regenerative Air Preheaters

**P. C. Mioralli^{1*}, M. A. B. Da Silva¹, E. Avallone¹, P. H. Palota¹
and P. S. G. Natividade¹**

¹*Federal Institute of São Paulo – IFSP, Campus Catanduva, Brazil.*

Authors' contributions

This work was carried out in collaboration among all authors. Authors PCM and MABDS designed the study and developed the computer program. Authors EA and PHP interpreted the results and wrote the first draft of manuscript. Author PSGN managed the literature searches. All authors read and approved the final manuscript.

Article Information

DOI: 10.9734/JENRR/2019/V2i430083

Editor(s):

(1) Dr. Salisu Muhammad Lawan, Department of Electrical and Electronics Engineering, Kano University of Science and Technology (KUST) Wudil, Nigeria.

Reviewers:

- (1) Fateh Mebarek Oudina, Skikda University, Algeria.
- (2) Yahaya Shagaiya Daniel, Kaduna State University, Nigeria.
- (3) Raheel Muzzammel, University of Lahore, Pakistan.

Complete Peer review History: <http://www.sdiarticle3.com/review-history/48540>

Received 30 January 2019

Accepted 15 April 2019

Published 25 April 2019

Original Research Article

ABSTRACT

A computational analysis in a rotary regenerative air preheater subject to pre-established mass flow rate is performed. The heat transfer rate, the pressure drop and the outlet temperatures of gas streams are calculated from different matrix porosity values. The fluid flow and the convective heat transfer coefficient are determined from correlations. The total heat transfer is obtained using the Effectiveness-NTU method specific to regenerative air preheaters. Three typical regenerative air preheaters with both streams under the laminar flow regime are investigated. A range of porosity values that provide good thermal exchange and low pressure drop in the equipment is chosen for each examined air preheater. The behavior of the outlet temperatures of each gas stream as function of porosity is also analyzed. The results show that the porosity ranges shorten when the typical pressured drop values for each regenerative air preheater are introduced in the analysis. In addition, the behavior of the outlet temperatures is compatible with the behavior of the heat transfer rate as the porosity changes.

*Corresponding author: E-mail: mioralli@ifsp.edu.br;

Keywords: Regenerative air preheater; heat transfer; pressure drop; simulation.

NOMENCLATURE

A	: Free flow cross-sectional area, m^2
A_m	: Matrix cross-sectional area, m^2
A_T	: Total cross-sectional frontal area ($A + A_m$), m^2
A_{tr}	: Heat exchange area, m^2
C	: Heat capacity rate of fluids, W/K
C_r	: Matrix heat capacity rate, W/K
C_r^*	: Matrix heat capacity rate ratio on the cold or hot side
c_p	: Specific heat of gas under constant pressure, $J/kg K$
c_m	: Specific heat of matrix, $J/kg K$
D_h	: Hydraulic diameter, m
e	: Thickness of the plates that constitute the matrix channels, m
f	: Darcy friction factor
h	: Convective heat transfer coefficient, $W/m^2 K$
k	: Thermal conductivity, W/mK
L	: Length of matrix, m
\dot{m}	: Gas mass flow rate, kg/s
m_m	: Mass of matrix, kg
n	: Rotational speed, rpm
NTU	: Number of heat transfer units on the cold or hot side
Nu	: Nusselt number
P	: Periphery of the channel, m
Pr	: Prandtl number
Q	: Heat transfer rate, W
Re	: Reynolds number
r_h	: Hydraulic radius ($D_h/4$), m
T	: Temperature, K
V	: Fluid velocity in the channel, m/s

GREEK SYMBOLS

μ	: Dynamic viscosity, Ns/m^2
ε_0	: Effectiveness of counterflow heat exchanger
ε_r	: Regenerator effectiveness
φ_r	: Correction factor
ρ	: Fluid density, kg/m^3
σ	: Porosity
ΔP	: Distributed pressure drop, Pa

SUBSCRIPTS

i	: Inlet
o	: Outlet
c	: Cold

h : Hot
min : Minimum
max : Maximum

1. INTRODUCTION

Regenerative air preheater is used in many heat recovery systems. Its range of applications encompasses refrigeration systems, ventilation plants, thermal comfort, power plant boilers, recovery of waste thermal energy and a number of situations where the availability of the energy does not chronologically coincide with demand [1].

Over the years, researchers have focused efforts on improving this heat exchanger due to some of its advantages such as compactness, efficiency, economy and high flexibility. The studies found in the literature incorporate different aspects of the equipment. The pioneer works about the regenerative air preheater were essentially experimental with investigations that mainly included the effectiveness, the thermal exchange and the pressure drop [2–5]. Later studies include aspects of the equipment such as mathematical modeling and numerical analysis [6-9], mass transfer [10-13], leakage control [14-16], thermodynamic analysis [17-19], rotational speed of the matrix [20-21] and geometry of matrix ducts [22-25].

Groups of researchers have also been conducted recent studies about regenerative preheaters. Wang et al. [26] developed the thermal hydraulic calculation program integrated with the multi-objective and single-objective genetic algorithms to perform design optimizations of regenerative air preheaters used in the coal-fired power plants. Herraiz et al. [27] investigated the use of rotary regenerative heat exchangers for the dry cooling of flue gases in combined cycle gas turbine plants equipped with post-combustion carbon capture. Sheng and Fang [28] experimentally investigated the effect of moisture on the air cleaning performance of a desiccant wheel with the objective to guide practical operation of clear air heat pump. Mohammadian Korouyeh et al. [29] evaluated the heating, cooling and electrical demands of a residential tower for Iran various weather conditions and the outlet air condition of the desiccant wheel was modeled based on the operational parameters by applying genetic algorithm. Kwiczala and Wejkowski [30] verified the effectiveness of the hybrid flue gas denitrification system which involved the

retrofitting for selective catalytic reduction material into a regenerative rotary air heater. The intent of the study was to provide a platform where the technology can be implemented on full scale air preheaters. Nguyen and Oh [31] evaluated and compared the heat transfer performance of a rotary regenerators made of metals and polymers. The rotary regenerator was used to preheat incoming fresh air with waste heat recovered from exhaust flue gas in a thermal power plant. Chen et al. [32] proposed a different configuration of desiccant dehumidification process in which a low energy cost dehumidification process using cascading desiccant wheels that can produce dehumidified air with a dew point of $-40 \sim 0^{\circ}\text{C}$ was considered. Bu et al. [33] presented the detailed analysis of the overall operation and performance of the novel rotary air preheater system and the effects of the operational and structural parameters by means of a numerical finite difference method. Jiang et al. [34] evaluated the operation of air preheater from the influence of denitrification system on the operation of air preheater, the calculation of air leakage rate of air preheater and the evaluation of low temperature corrosion for air preheater. Zhang et al. [35] established a three-dimensional numerical model of quad-sectional air preheater based on FLUENT software. The accuracy of the model was verified by comparing with actual operation conditions. Sha et al. [36] proposed a new framework of data-driven state monitoring approach for the thermal power plant devices and identified various air leakage states accurately and efficiently on operating data of a rotary air preheater. Zhang et al. [37] proposed an online applicable approach to estimate the direct leakage of the rotary air preheater based on temperature distribution modeling for improving the safe and economic operation of the unit. Nourozi et al. [38] investigated the energy performance of a mechanical ventilation with heat recovery system combined with an air preheater in a multi-family house and a sensitivity analysis of energy wheel efficiency was implemented in different cases. Shi et al. [39] proposed a comprehensive approach for optimization of soot-blowing of air preheater in a coal-fired power plant boiler. The approach combined online modeling of heat transfer efficiency to monitor the fouling level, statistical fitting to characterize the dynamics of cleanliness

factor, and soot-blowing optimization aiming at steam consumption conservation.

There are many studies carried out concerning to regenerative air preheater but analysis from the matrix porosity are found in a few works [40-44]. However, a literature review reveals contemporary studies involving energy transport in porous elements associated with other component or equipment, such as investigations covering thermal analysis of nanofluids flow over permeable stretching sheets [45-60]. The present work focuses on the porous matrix of a rotary regenerative air preheater. The goal is simultaneously to analyze the effects of matrix porosity on heat transfer and pressure drop in the equipment with both gas streams. The difference to previous studies as well as the contribution of the present study is this simultaneous analysis from matrix porosity. The main intention with this study is to select a range of porosity values that provide good thermal exchange and low pressure drop in the air preheater and analyze the behavior of the outlet temperatures of each gas stream as function of porosity.

2. PROBLEM DESCRIPTION AND METHODOLOGY

2.1 Characterization of the Regenerative Air Preheater

The schematic of the regenerative air preheater is show in Fig. 1. Two gas streams are introduced counter flow-wise through the parallel ducts of the air preheater. Cold gas is injected inside one duct and hot gas inside the other. The porous matrix, that stores energy, continuously rotates through these parallel ducts. The matrix receives heat from the hot gas on one side and transfers this energy to the cold gas on the other side. The matrix channels were assumed

smooth. The fluid velocity was considered constant inside each channel.

Some geometric parameters can be expressed based on Fig. 1. The total frontal cross-sectional area A_T is determined by the sum of the free flow cross-sectional area A and the matrix cross-sectional area A_m of the air preheater

$$A_T = A + A_m \quad (1)$$

The matrix porosity σ is defined by the ratio between A and A_T

$$\sigma = \frac{A}{A_T} \quad (2)$$

The hydraulic radius r_h is defined by the ratio between A and the perimeter P of the plates that compose the matrix. The matrix perimeter can be written as function of the matrix cross-sectional area A_m

$$r_h = \frac{D_h}{4} = \frac{A}{P} \quad (3)$$

$$P = \frac{A_m}{(e/2)} \quad (4)$$

where D_h and e are the matrix duct hydraulic diameter and the matrix duct wall thickness, respectively.

The porosity and the hydraulic radius are dependent on each other and influence the thermal exchange in the regenerative air preheater. The hydraulic radius can be written as function of the porosity and the matrix duct wall thickness from the definitions above and algebraic manipulations

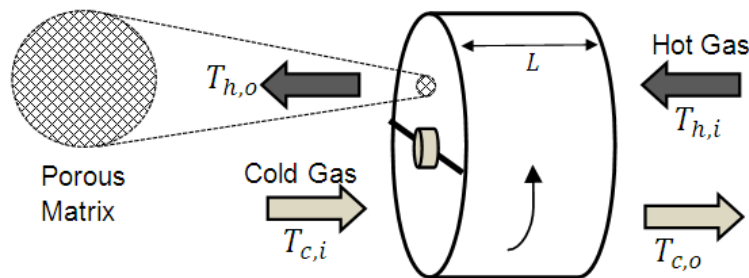


Fig. 1. Schematic of the regenerative air preheater

Table 1. Matrix properties of the regenerative air preheater

Material	c_m (J/kg K)	ρ_m (kg/m ³)
2024-T6 aluminum	875	2,770
AISI 1010 alloy carbon steel	434	7,832

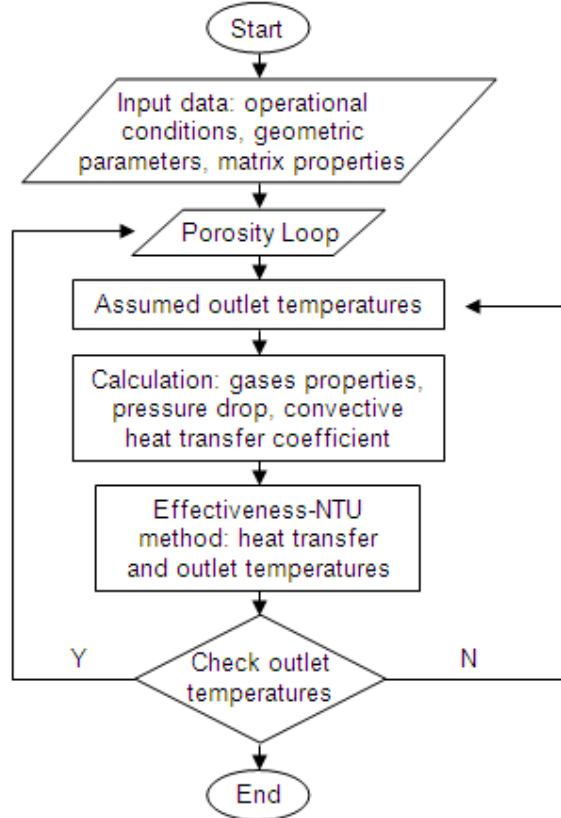


Fig. 2. Schematic diagram of the calculation process

Table 2. Comparison of the present data with Petrobras field data

Outlet temperature (°C)	Present work	Field data	Difference
$T_{c,o}$	441.26	405.65	0.088
$T_{h,o}$	160.51	194.27	0.170

$$r_h = \frac{\sigma}{1 - \sigma} \left(\frac{e}{2} \right) \quad (5)$$

The hydraulic radius is an important parameter and its use is justified in the correlations for friction factor and Nusselt number. Since the geometric characteristics of the regenerator are known, the heat transfer in the equipment can be calculated using the Effectiveness-NTU method for rotary regenerators.

2.2 Effectiveness-NTU Method for Regenerative Air Preheaters

The Effectiveness-NTU method for regenerative air preheaters [61] consists of calculating the effectiveness ϵ_0 of a conventional counterflow heat exchanger and correcting this effectiveness by a correction factor ϕ_r , that takes into account the rotational speed and the matrix heat capacity

rate of the exchanger. Thus, the effectiveness of the regenerator ε_r is given by

$$\varepsilon_r = \varepsilon_0 \varphi_r \quad (6)$$

The effectiveness ε_0 of a conventional counterflow heat exchanger is defined by

$$\varepsilon_0 = \frac{1 - \exp[-NTU(1 - C^*)]}{1 - C^* \exp[-NTU(1 - C^*)]} \quad (7)$$

where C^* is the ratio between the fluids heat capacity rates and NTU is the number of heat transfer units defined as follows

$$C^* = \frac{C_{min}}{C_{max}} \quad (8)$$

$$NTU = \frac{1}{C_{min}} \left[\frac{1}{(1/hA_{tr})_c + (1/hA_{tr})_h} \right] \quad (9)$$

where h is the convective heat transfer coefficient and A_{tr} is the matrix thermal exchange area on the side of the hot or cold stream. The parameters C_{min} and C_{max} correspond to the minimum and maximum values of the fluids heat capacity rates.

The correction factor φ_r in Eq. (6) is given by

$$\varphi_r = \frac{1}{9C_r^{*1.93}} \quad (10)$$

$$C_r^* = \frac{C_r}{C_{min}} \quad (11)$$

$$C_r = \frac{n}{60} m_m c_m \quad (12)$$

where C_r is the matrix heat capacity rate, n is the matrix rotational speed, m_m is the matrix mass and c_m is the specific heat of matrix.

Finally, the total heat transfer Q in the air preheater is obtained in the same way as the Effectiveness-NTU method for conventional heat exchangers

$$Q = \varepsilon_r Q_{max} \quad (13)$$

$$Q_{max} = C_{min} (T_{h,i} - T_{c,i}) \quad (14)$$

where Q_{max} is the maximum possible heat transfer and the term between parenthesis corresponds to the difference between the inlet temperature of the hot stream and the inlet temperature of the cold stream.

2.3 Hydrodynamic and Thermal Analysis

The hydrodynamic and thermal analysis are performed for each gas stream. The pressure drop in the matrix ducts and the convective heat transfer coefficient are obtained from correlations for Darcy friction factor f and Nusselt number Nu . Correlations for smooth ducts with circular cross-sectional area were used based on the hydraulic diameter of matrix ducts for laminar flow regime. The correlations take into account hydrodynamically fully developed flow with thermal entrance length and constant wall temperature boundary condition.

$$f = \frac{64}{Re_{D_h}} \quad (15)$$

$$Nu = 3.66 + \frac{0.0668 \left(\frac{D_h}{L} \right) Re_{D_h} Pr}{1 + 0.04 \left[\left(\frac{D_h}{L} \right) Re_{D_h} Pr \right]^{\frac{2}{3}}} \quad (16)$$

where L is the length of matrix, Re_{D_h} is the Reynolds number and Pr is the Prandtl number.

The distributed pressure drop ΔP is given by equation of Darcy-Weisbach and the convective heat transfer coefficient h is expressed in terms of Nusselt number

$$\Delta P = f \rho \frac{L}{D_h} \frac{V^2}{2} \quad (17)$$

$$h = \frac{Nu k}{D_h} \quad (18)$$

Where V , ρ and k are the fluid velocity, the fluid density and the fluid thermal conductivity, respectively.

2.4 Fluid and Matrix Properties

The fluid properties were obtained at the average temperature of each gas stream. The fluid

density for gases with moderate values of pressure and temperature is well represented by the equation of state of an ideal gas

$$\rho = \frac{p}{RT} \quad (19)$$

Where p is the pressure of fluid, T is the average temperature of gas stream and R is the ideal gas constant. The values of air atmospheric pressure $p = 10^5 Pa$ and ideal gas constant for air $R = 287 Nm/kgK$ were assumed.

The dynamic viscosity μ and the thermal conductivity k of fluids can be approximated by the Sutherland equations [62] as follows

$$\frac{\mu}{\mu_0} \approx \left(\frac{T}{T_0} \right)^{3/2} \frac{T_0 + S}{T + S} \quad (20)$$

$$\frac{k}{k_0} \approx \left(\frac{T}{T_0} \right)^{3/2} \frac{T_0 + S}{T + S} \quad (21)$$

Where S is the Sutherland constant temperature, which is characteristic of each gas. Considering air $S = 111 K$ for dynamic viscosity and $S = 194 K$ for thermal conductivity. The parameters T_0 , μ_0 and k_0 are reference constants whose values are $T_0 = 273 K$, $\mu_0 = 1.716 \cdot 10^{-5} Pa \cdot s$ and $k_0 = 0.0241 W/mK$ for air.

The specific heat of gas under constant pressure c_p is obtained by a polynomial equation [63] for several gases in the temperature range between 300 and 1,000 K

$$\frac{c_p}{R} = \alpha_0 + \beta_0 T + \gamma_0 T^2 + \delta_0 T^3 + \lambda_0 T^4 \quad (22)$$

where $\alpha_0 = 3.653$, $\beta_0 = -1.337 \cdot 10^{-3}$, $\gamma_0 = 3.294 \cdot 10^{-6}$, $\delta_0 = -1.913 \cdot 10^{-9}$ and $\lambda_0 = 0.2763 \cdot 10^{-12}$ are the air constants.

The Prandtl number Pr is obtained from the ratio between some fluid properties, as follow

$$Pr = \frac{\mu c_p}{k} \quad (23)$$

The matrix properties of the regenerative air preheater were assumed constant. The AISI 1010 low alloy carbon steel and the 2024-T6 aluminum alloy materials were considered for the matrix. Table 1 shows the matrix properties used in this study, where c_m and ρ_m are the specific heat and the density of matrix, respectively.

2.5 Computer Program

A computer program written in C programming language was developed for the simulation of regenerative air preheater. The Dev-C++ software was used for compilation and recording results. Three typical sizes of equipment were simulated: Small, medium-sized and large. The material AISI 1010 low alloy carbon steel was used for the medium-sized and the large heat exchangers in the simulations. The 2024-T6 aluminum alloy was used for the small air preheater. The total heat transfer in the air preheater, the pressure drop and the outlet temperatures of gas streams were calculated for different porosity levels of the matrix from the prescribed mass flow rate for each gas stream. The other geometric parameters of the equipment were fixed.

An iterative process was used to obtain the fluid flow and the heat transfer. An outlet temperature values of each stream was assumed at the beginning of this process. Then, the fluid properties were evaluated at the average temperature of each gas stream. Based on these properties, the fluid flow and the heat transfer were obtained from correlations and the Effectiveness-NTU method for regenerative air preheaters. The iterative process continued until convergence of the outlet temperatures for both streams. The whole process was repeated for each assumed matrix porosity value. The subrelaxation factor of 0.5 was used to the convergence of the outlet temperature values. The tolerance for convergence iterative procedure was adjusted as 10^{-3} for the outlet temperatures. The calculations were performed considering the steady-periodic condition of the regenerator, indicating that the temperatures no longer changed in any angular or axial position of the matrix. The schematic diagram of the calculation process is shown in Fig. 2.

In order to check the reliability of the developed computer program, the outlet temperatures of gas streams were calculated at a medium-sized rotary regenerator with corrugated ducts. The

results were compared with field data of a regenerative air preheater in operation at the PETROBRAS petroleum refinery of Paulínia city. The operational conditions and geometric dimensions of this PETROBRAS air preheater are found in Mioralli [64]. Table 2 shows the comparison between the results of the present study and the field data. It is observed that the results are in reasonable agreement with a greater difference for the hot outlet temperature values.

3. RESULTS AND DISCUSSION

The input data of the developed computer program are listed in Table 3. The operational conditions of the regenerative air preheaters are based on information from literature and industry. The simulations were carried out from different porosity values in the range of 0.2 up to the last value required to preserve both gas streams inside the equipment under the laminar flow regime.

3.1 Thermal Exchange and Pressure Drop Analysis

Graphs with the heat transfer rate and the pressure drop as function of porosity are shown for each regenerative air preheater. The heat transfer rate increases and the pressure drop decreases as the porosity increases for all analyzed cases. In this study is assumed as good thermal exchange a heat transfer value whose reduction is less than 30% when compared with the highest heat transfer rate

(obtained for $\sigma = 0.2$) in the simulated cases. In addition, the typical low pressure drop values for each regenerative air preheater are supposed according reference [65].

Fig. 3 shows the total heat transfer in the small regenerative air preheater and the pressure drop of both gas streams as function of matrix porosity. The heat transfer in the equipment begins to decrease more significantly for $\sigma \geq 0.5$. The low pressure drop for both gas streams occurs for $\sigma \geq 0.6$. Based on Fig. 3, the range $0.60 \leq \sigma \leq 0.75$ could be chosen as the porosity values that provide good thermal exchange and low pressure drop in the small regenerative air preheater. Porosity values $\sigma \geq 0.75$ implies a reduction in the heat transfer rate almost 30% when compared to the highest heat transfer rate $Q \cong 20.5 kW$ for $\sigma = 0.2$ as observed in Fig. 3. The range $0.60 \leq \sigma \leq 0.75$ corresponds to pressure drop values between $650 Pa > \Delta P > 100 Pa$ as observed in Fig. 4, which shows the pressure drop versus porosity for $\sigma \geq 0.6$. However, the typical pressure drop values for the small regenerative air preheater are $\Delta P < 200 Pa$ [65] suggesting porosity values $\sigma \geq 0.71$. Considering this, another porosity range must be chosen as the appropriate for good thermal exchange and low pressure drop. So, the range $0.71 \leq \sigma \leq 0.75$ can be chosen as suitable for good thermal exchange and low pressure drop in the small regenerative air preheater taking into account the typical pressure drop values and the reduction in the heat transfer rate less than 30%.

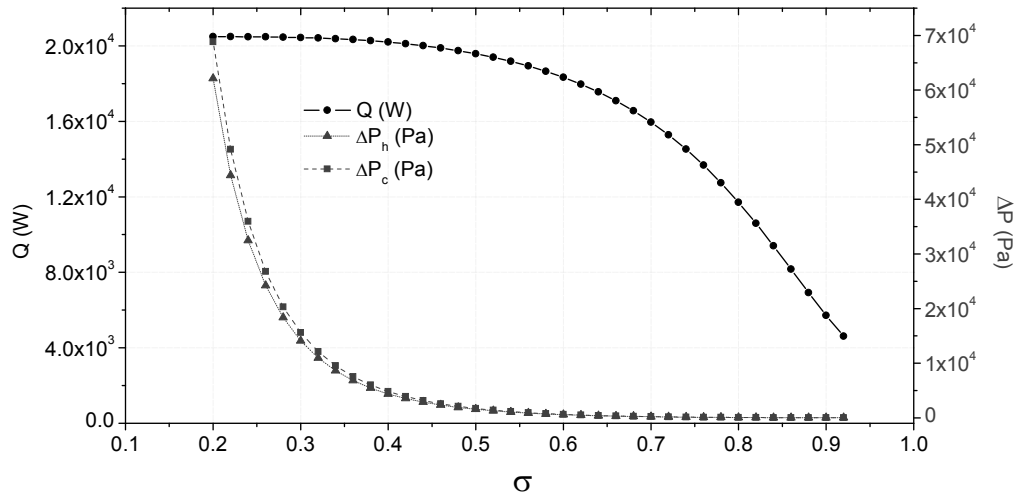


Fig. 3. Heat transfer and pressure drop versus porosity for small regenerative air preheater

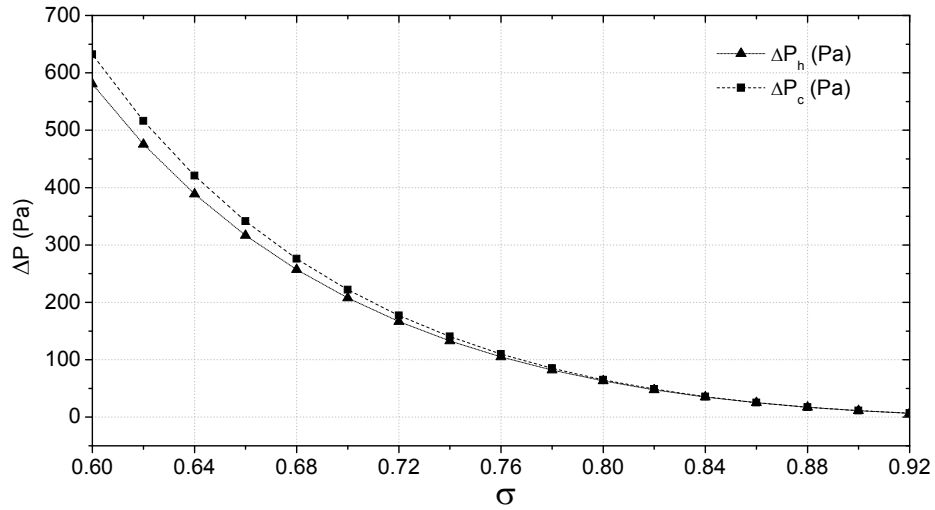


Fig. 4. Pressure drop versus porosity for small regenerative air preheater considering $\sigma \geq 0.6$

Table 3. Input data for computer program of typical regenerative air preheaters

Air preheater	L (m)	e (m)	D (m)	n (rpm)	Inlet Temp. (°C)		Flow rate (kg/s)	
					$T_{h,i}$	$T_{c,i}$	\dot{m}_h	\dot{m}_c
Small	0.2	0.00035	0.7	8	50	20	0.68	0.76
Medium-sized	1.5	0.00050	6.0	3	450	80	39.00	62.00
Large	3.5	0.00060	15.0	2	600	150	292.50	411.30

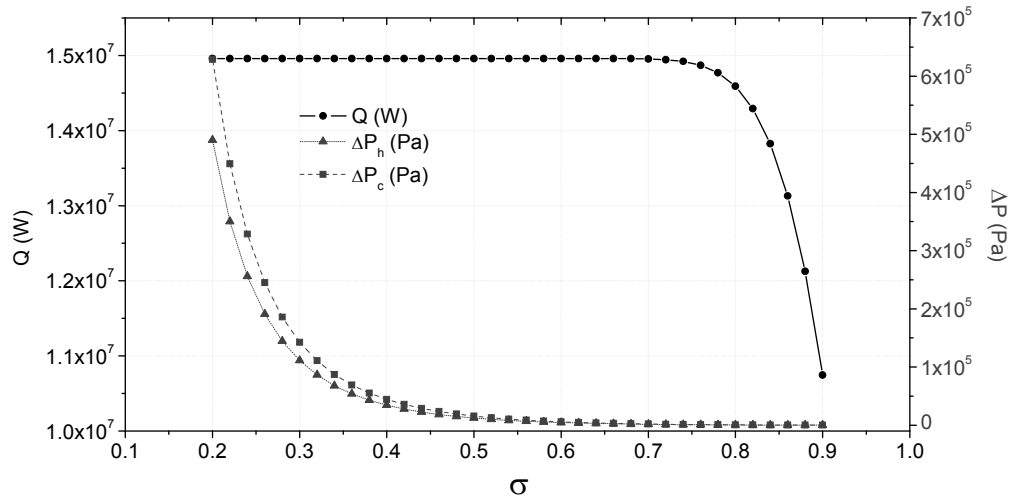


Fig. 5. Heat transfer and pressure drop versus porosity for medium-sized regenerative air preheater

Fig. 5 shows the total heat transfer in the medium-sized regenerative air preheater and the pressure drop of both gas streams as function of matrix porosity. In this case, the heat transfer rate in the equipment begins to decrease considerably for $\sigma \geq 0.75$ and the low pressure

drop for both gas streams arises for $\sigma \geq 0.7$. An analysis on Fig. 5 indicates that the range $0.70 \leq \sigma \leq 0.90$ could be appropriate for good thermal exchange and low pressure drop in the medium-sized regenerative air preheater. The porosity $\sigma = 0.90$ implies a reduction in the heat

transfer rate closer to 28% when compared to the highest heat transfer rate $Q \cong 15 MW$ for $\sigma = 0.2$ as observed in Fig. 5. The porosity values $\sigma > 0.90$ imply turbulent flow regime for at least one of the gas streams. The range $0.70 \leq \sigma \leq 0.90$ corresponds to pressure drop values between $2000 Pa > \Delta P > 90 Pa$ as indicated by Fig. 6, which shows the pressure drop versus porosity for $\sigma \geq 0.7$. Nonetheless, the typical pressure drop values for the medium-sized regenerative air preheater are $\Delta P < 350 Pa$ [65] suggesting porosity values $\sigma \geq 0.84$. Thus, considering the typical pressure drop values and the reduction in the heat transfer rate less than

30% in the medium-sized regenerative air preheater, the range $0.84 \leq \sigma \leq 0.90$ can be chosen as suitable for good thermal exchange and low pressure drop in this case.

Analogously to the cases for small and medium-sized regenerative air preheaters, Fig. 7 shows the total heat transfer in the large regenerative air preheater and the pressure drop of both gas streams as function of matrix porosity. The heat transfer rate in the equipment greatly decreases for $\sigma \geq 0.77$ and the low pressure drop for both gas streams occurs for $\sigma \geq 0.7$. An analysis on Fig. 7 indicates that the range $0.70 \leq \sigma \leq 0.90$

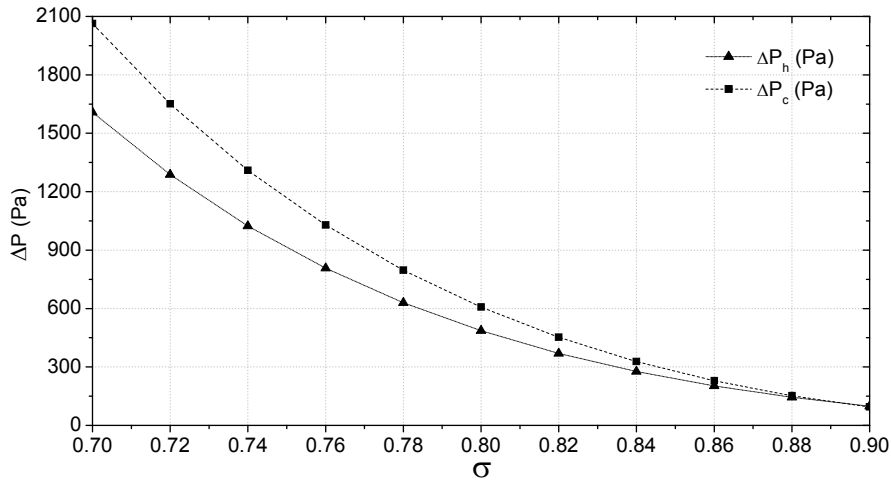


Fig. 6. Pressure drop versus porosity for medium-sized regenerative air preheater considering $\sigma \geq 0.70$

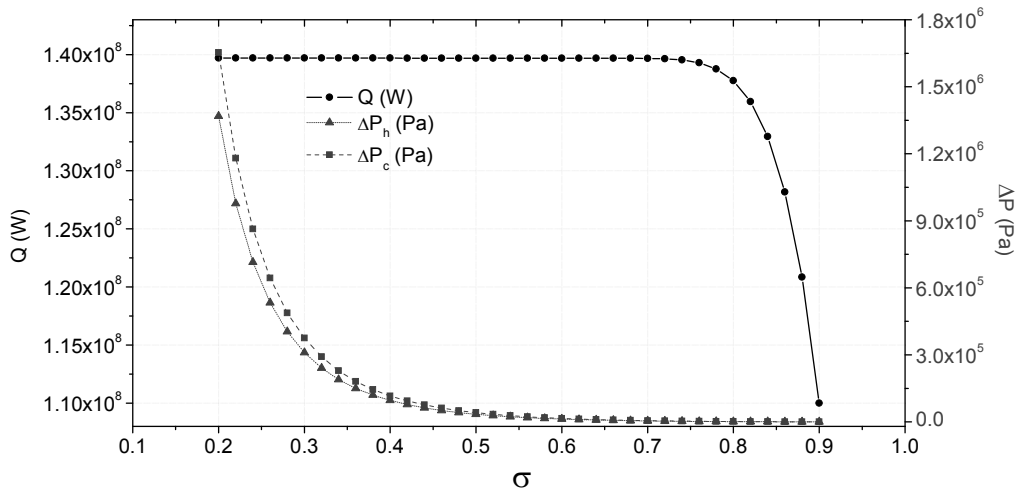


Fig. 7. Heat transfer and pressure drop versus porosity for large regenerative air preheater

could be chosen as the porosity values that provide good thermal exchange and low pressure drop in the large regenerative air preheater. The porosity $\sigma = 0.90$ implies a reduction in the heat transfer rate closer to 22% when compared to the highest heat transfer rate $Q \cong 0.14 \text{ GW}$ for $\sigma = 0.2$ as observed in Fig. 7. The porosity values $\sigma > 0.90$ imply turbulent flow regime for at least one of the gas streams. The range $0.70 \leq \sigma \leq 0.90$ corresponds to pressure drop values between $5500 \text{ Pa} > \Delta P > 200 \text{ Pa}$ as indicated by Fig. 8, which shows the pressure drop versus porosity for $\sigma \geq 0.7$. However, the typical pressure drop values for the large regenerative air preheater are $\Delta P < 600 \text{ Pa}$ [65]

suggesting porosity values $\sigma \geq 0.86$. Finally, the range $0.86 \leq \sigma \leq 0.90$ can be chosen as suitable for good thermal exchange and low pressure drop in the large regenerative air preheater taking into account the typical pressure drop values and the reduction in the heat transfer rate less than 30%.

The results shows that the selected porosity ranges shorten when the typical pressured drop values for each regenerative air preheater are introduced in the analysis. Furthermore, a simultaneous analysis on Figs. 3 to 8 shows that the chosen ranges of porosity values that provide good thermal exchange and low pressure drop

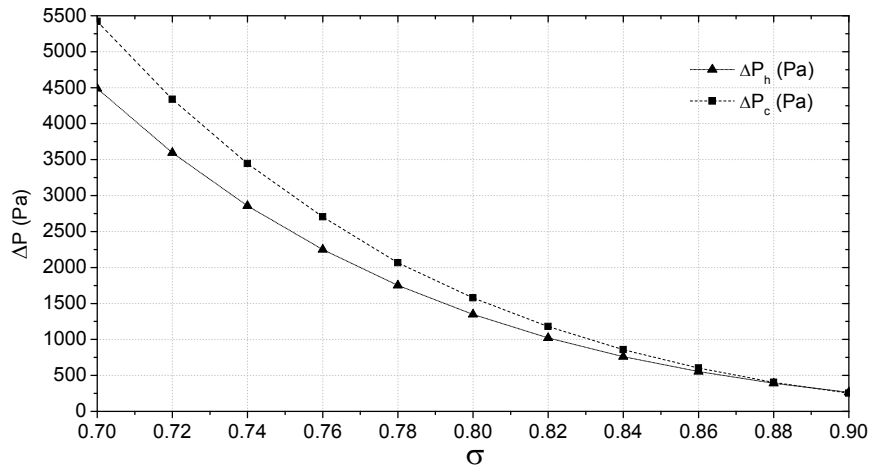


Fig. 8. Pressure drop versus porosity for large regenerative air preheater considering $\sigma \geq 0.70$

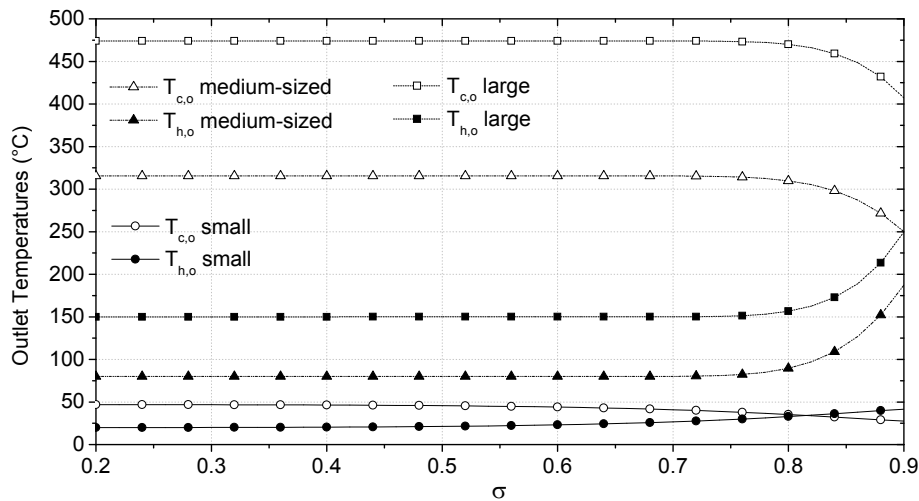


Fig. 9. Outlet temperatures versus porosity for small, medium-sized and large regenerative air preheaters

moves to the right on the abscissa axis as the dimensions and typical operational conditions of the regenerative air preheaters increase. It is also observed that the chosen porosity ranges for the three simulated cases are relatively narrow.

The porosity ranges could be extended if higher pressured drop values in the heat exchanger were considered. However, this would imply higher pumping power and energy costs. On the other hand, the porosity ranges could be shortened if the desired reduction in the heat transfer rate was less than 20% or 15% when compared to the highest heat transfer obtained for $\sigma = 0.2$.

3.2 Outlet Temperatures Analysis

The behavior of the outlet temperatures of cold ($T_{c,o}$) and hot ($T_{h,o}$) streams as function of matrix porosity is shown in Fig. 9 for the three typical regenerative air preheaters. The outlet temperatures remain approximately equal to $\sigma \leq 0.60$ for small heat exchanger and $\sigma \leq 0.72$ for medium-sized and large regenerative air preheaters because these porosity values imply a larger thermal exchange area and high heat transfer rate. The hot stream experience the greatest temperature change and the hot outlet temperature is closer to the cold inlet temperature. The mass flow rate strongly contributes to this since the mass flow rate of the hot stream is lower than that of the cold stream for all cases. On the other hand, the cold outlet temperature is lower than the hot inlet temperature for the three simulated preheaters taking into account the porosity values that maintain the outlet temperatures approximately equal: $T_{c,o} \cong 0.9 T_{h,i}$ for the small exchanger, $T_{c,o} \cong 0.7 T_{h,i}$ for the medium-sized air preheater and $T_{c,o} \cong 0.8 T_{h,i}$ for the large equipment. These outlet temperature values are meaningful but the pressure drop is high under these operational conditions. As a comparison, the cold outlet temperatures within the porosity range that provides good thermal exchange and low pressure drop are $T_{c,o} \cong 0.8 T_{h,i}$ (with $\sigma = 0.74$), $T_{c,o} \cong 0.65 T_{h,i}$ (with $\sigma = 0.86$) and $T_{c,o} \cong 0.7 T_{h,i}$ (with $\sigma = 0.88$) for the small, medium-sized and large regenerative air preheaters, respectively. These values corresponds to a reduction closer to 11%, 7% and 12% when compared to related cases with cold outlet temperatures approximately equal as porosity changes.

Lastly, the results shown in Fig. 9 are compatible with those of Figs. 3, 5 and 7. The difference between the cold and hot outlet temperatures begins to decrease in Fig. 9 for porosity values close to those in which the heat transfer rate starts to decrease in Figs. 3, 5 and 7.

4. CONCLUSION

Three typical regenerative air preheaters were computationally investigated from the pre-established mass flow rate for each gas stream of the equipment and different matrix porosity values. The outlet temperatures of gas streams were also analyzed as function of matrix porosity. The conclusions can be summarized as follows:

- A porosity range that provide good thermal exchange and low pressure drop was chosen for each simulated typical regenerative air preheater.
- The amplitude of porosity ranges is determined by the desired limits for the heat transfer rate and the pressure drop in the equipment. The porosity ranges shorten when the typical pressured drop values for each regenerative air preheater are introduced in the analysis.
- The selected ranges of porosity values that provide good thermal exchange and low pressure drop moves to the right on the porosity axis as the dimensions and typical operational conditions of the regenerative air preheaters increase. Moreover, the chosen porosity ranges for the three simulated cases are relatively narrow.
- The behavior of the outlet temperatures is compatible with the behavior of the heat transfer rate for the three simulated regenerative air preheaters. The difference between the cold and hot outlet temperatures begins to decrease for porosity values close to those in which the heat transfer rate starts to decrease.
- The results can help define operational conditions of regenerative air preheaters in search of better performance.

COMPETING INTERESTS

Authors have declared that no competing interests exist.

REFERENCES

1. Bae YL. Performance of rotary regenerative heat exchanger - A numerical

- simulation. Doctoral Thesis, Oregon State University; 1986.
2. Karlsson H, Holm S. Heat transfer and fluid resistances in ljungstrom regenerative-type air preheaters. Transactions of the ASME. 1943;65:61-72.
 3. London AL, Kays WM. The gas-turbine regenerator – The use of compact heat-transfer surfaces. Transactions of the ASME. 1950;72:611-621.
 4. Harper DB, Rohsenow WM. Effect of rotary regenerator performance on gas-turbine-plant performance. Transactions of the ASME. 1953;75:759-765.
 5. Lambertson TJ. Performance factors of a periodic-flow heat exchanger. Transactions of the ASME. 1958;80:586-592.
 6. Van Den Bulck E, Mitchell J, Klein SA. Design theory for rotary heat and mass exchangers – I: Wavy analysis of rotary heat and mass exchangers with infinite transfer coefficients. International Journal of Heat and Mass Transfer. 1985;28:1575-1586.
 7. Ghodsipour N, Sadrameli M. Experimental and sensitivity analysis of a rotary air preheater for the flue gas heat recovery. Applied Thermal Engineering. 2003;23: 571-580.
 8. Wu Z, Melnik RVN, Borup F. Model-based analysis and simulation of regenerative heat wheel. Energy and Buildings. 2006; 38:502-514.
 9. Nóbrega CEL, Brum NCL. Local and average heat transfer coefficients for rotary heat exchangers. Proceedings of COBEM; 2007. Paper Code 1119.
 10. Tanthapanichakoon W, Prawarnpit A. New simple mathematical model of a honeycomb rotary absorption-type dehumidifier. Chemical Engineering Journal. 2002;86:11-15.
 11. Sphaier LA, Worek WM. Analysis of heat and mass transfer in porous sorbents used in rotary regenerators. International Journal of Heat and Mass Transfer. 2004; 47:3415-3430.
 12. Harshe YM, Utikar RP, Ranade VV, Pahwa D. Modeling of Rotary Desiccant Wheels. Chemical Engineering & Technology. 2005;28(12):1473-1479.
 13. Sphaier LA. Unified Formulation for Heat and Mass Transfer in Rotary Regenerators. Proceedings of COBEM; 2007. Paper Code 1290.
 14. Skiepko T. Experimental results concerning seal clearances in some rotary heat exchangers. Heat Recovery Systems and CHP. 1988;8:577-581.
 15. Skiepko T. Method of monitoring and measuring seal clearances in a rotary heat exchanger. Heat Recovery Systems and CHP. 1988;8:469-473.
 16. Shah RK, Skiepko T. Influence of leakage distribution on the thermal performance of a rotary regenerator. Thermal Engineering. 1999;19:685-705.
 17. Skiepko T. Irreversibilities associated with a rotary regenerator and the efficiency of a steam power plant. Heat Recovery Systems and CHP. 1990;10:187-211.
 18. Jassim RK, Habeebullah BA, Habeebullah AS. Exergy analysis of carryover leakage irreversibilities of a power plant regenerative air heater. Proceedings Institution of Mechanical Engineers. Part A: Journal of Power and Energy. 2004;218:23-32.
 19. Shang W, Besant RW. Effects of manufacturing tolerances on regenerative exchanger number of transfer units and entropy generation. Journal of Engineering for Gas Turbines and Power. 2006;128: 585-598.
 20. Büyükalaca O, Yilmaz T. Influence of rotational speed on effectiveness of rotary-type heat exchanger. International Journal of Heat and Mass Transfer. 2002;38:441-447.
 21. Worsøe-Schmidt P. Effect of fresh air purging on the efficiency of energy recovery from exhaust air in rotary regenerators. Rev. Int. Froid. 1991;14:233-239.
 22. Sunden B, Karlsson I. Enhancement of heat transfer in rotary heat exchangers by streamwise-corrugated flow channels. Experimental Thermal and Fluid Science. 1991;4:305-316.
 23. Utriainen E, Sunden B. numerical analysis of a primary surface trapezoidal cross wavy duct. International Journal of Numerical Methods for Heat & Fluid Flow. 2000;10(6):634-648.
 24. Comini G, Nonino C, Savino S. Effect of space ratio and corrugation angle on convection enhancement in wavy channels. International Journal of Numerical Methods for Heat & Fluid Flow. 2003;13(4):500-519.
 25. Zhang L. Laminar flow and heat transfer in plate-fin triangular ducts in thermally developing entry region. International Journal of Heat and Mass Transfer. 2007; 50:1637-1640.

26. Wang L, Bu Y, Li D, Tang C, Che D. Single and multi-objective optimizations of rotary regenerative air preheater for coal-fired power plant considering the ammonium bisulfate deposition. *International Journal of Thermal Sciences*. 2019;136:52–59.
27. Herraiz L, Hogg D, Cooper J, Lucquiaud M. Reducing the water usage of post-combustion capture systems: The role of water condensation/evaporation in rotary regenerative gas/gas heat exchangers. *Applied Energy*. 2019;239:434–453.
28. Sheng Y, Fang L. Experimental analysis of the effect of moisture on air cleaning performance of desiccant wheel in a Clean Air Heat Pump. *Building and Environment*. 2019;147:551–558.
29. Mohammadian Korouyeh M, Saidi MH, Najafi M, Aghanajafi C. Evaluation of desiccant wheel and prime mover as combined cooling, heating, and power system. *International Journal of Green Energy*. 2019;16(3):256–268.
30. Kwiczala A, Wejkowski R. Hybrid technology of reduction of nitrogen oxides (NOx) in exhaust gases; Part 2-Numerical model of pilot scale regenerative rotary air heater (RAH) retrofited with selective catalyst reduction (SCR) modules. *E3S Web of Conferences*. 2019;82:01016.
31. Nguyen NV, Oh DW. Analysis of thermal performance of polymer rotary regenerator. *High Temperatures - High Pressures*. 2019;48(1-2):107-120.
32. Chen Q, Jones JR, Archer RH. A dehumidification process with cascading desiccant wheels to produce air with dew point below 0°C. *Applied Thermal Engineering*. 2019;148:78-86.
33. Bu Y, Wang L, Deng L, Che D. Technical and economical analysis of a novel rotary air preheater system. *Applied Thermal Engineering*. 2019;154:102-110.
34. Jiang L, Du L, Li Q. Operation condition evaluation and risk prediction of air preheater in coal-fired power plant. *IOP Conference Series: Earth and Environmental Science*. 2019;233:052002.
35. Zhang Q, Sun F, Chen C. Research on the three-dimensional wall temperature distribution and low-temperature corrosion of quad-sectional air preheater in larger power plant boilers. *International Journal of Heat and Mass Transfer*. 2019;128:739-747.
36. Sha P, Wu X, Shen J, Liu X, Wang M. Data-driven state monitoring of air preheater using density peaks clustering and evidential K-nearest neighbour classifier. *MATEC Web of Conferences*. 2019;272:01003.
37. Zhang X, Yuan J, Tian Z, Wang J. Estimation of the direct leakage of rotary air preheaters based on temperature distribution modeling. *International Journal of Heat and Mass Transfer*. 2019;134:119-130.
38. Nourozi B, Wang Q, Ploskić A. Energy and defrosting contributions of preheating cold supply air in buildings with balanced ventilation. *Applied Thermal Engineering*. 2019;146:180-189.
39. Shi Y, Wen J, Cui F, Wang J. An optimization study on soot-blowing of air preheaters in coal-fired power plant boilers. *Energies*. 2019;12(5): 958.
40. Mioralli PC, Ganzarolli MM. Temperature Distribution in a Rotary Heat Exchanger. *Proceedings of COBEM; 2005. Paper Code 0356*.
41. Mioralli PC, Ganzarolli MM. Influência da porosidade no desempenho de um regenerador rotativo. *Anais ENCIT*. 2006;CIT06-0549. Portuguese.
42. Mioralli PC, Ganzarolli MM. Optimal porosity of a rotary regenerator with fixed pressure drop. *Proceedings of ECOS*. 2007;1307-1314.
43. Mioralli PC, Ganzarolli MM. Thermal optimization of a rotary regenerator with fixed pressure drop. *Proceedings of ENCIT; 2008. Paper Code 7-5302*.
44. Mioralli PC, Ganzarolli MM. Thermal analysis of a rotary regenerator with fixed pressure drop or fixed pumping power. *Applied Thermal Engineering*. 2013;52: 187-197.
45. Daniel YS. Boundary layer stagnation point flow of a nanofluid over a permeable surface with velocity, thermal and solutal slip boundary conditions. *Journal of Applied Physical Science International*. 2015;4(4):237-252.
46. Daniel YS, Daniel SK. Effects of buoyancy and thermal radiation on MHD flow over a stretching porous sheet using homotopy analysis method. *Alexandria Engineering Journal*. 2015;54(3):705-712.
47. Daniel YS. Steady MHD. Laminar flows and heat transfer adjacent to porous stretching sheets using HAM. *American Journal of Heat and Mass Transfer*. 2015; 2(3):146-159.

48. Daniel YS. Presence of heat generation/ absorption on boundary layer slip flow of nanofluid over a porous stretching sheet. American Journal of Heat and Mass Transfer. 2015;2(1):15-30.
49. Daniel YS. Steady MHD boundary-layer slip flow and heat transfer of nanofluid over a convectively heated of a non-linear permeable sheet. Journal of Advanced Mechanical Engineering. 2016;3(1):1-14.
50. Daniel YS, Aziz ZA, Ismail Z, Salah F. Double stratification effects on unsteady electrical MHD mixed convection flow of nanofluid with viscous dissipation and Joule heating. Journal of Applied Research and Technology. 2017;15(5):464-476.
51. Daniel YS, Aziz ZA, Ismail Z, Salah F. Effects of thermal radiation, viscous and Joule heating on electrical MHD nanofluid with double stratification. Chinese Journal of Physics. 2017;55(3):630-651.
52. Daniel YS, Aziz ZA, Ismail Z, Salah F. Entropy analysis in electrical magneto-hydrodynamic (MHD) flow of nanofluid with effects of thermal radiation, viscous dissipation and chemical reaction. Theoretical and Applied Mechanics Letters. 2017;7(4):235-242.
53. Daniel YS, Aziz ZA, Ismail Z, Salah F. Entropy analysis of unsteady magneto-hydrodynamic nanofluid over stretching sheet with electric field. International Journal for Multiscale Computational Engineering. 2017;15(6):545-565.
54. Daniel YS. MHD laminar flows and heat transfer adjacent to permeable stretching sheets with partial slip condition. Journal of Advanced Mechanical Engineering. 2017; 4(1):1-15.
55. Daniel YS, Aziz ZA, Ismail Z, Salah F. Numerical study of Entropy analysis for electrical unsteady natural magnetohydrodynamic flow of nanofluid and heat transfer. Chinese Journal of Physics. 2017; 55(5):1821-1848.
56. Daniel YS, Aziz ZA, Ismail Z, Salah F. Thermal radiation on unsteady electrical MHD flow of nano fluid over stretching sheet with chemical reaction. Journal of King Saud University-Science; 2017.
57. Daniel YS, Aziz ZA, Ismail Z, Salah F. Effects of slip and convective conditions on MHD flow of nanofluid over a porous nonlinear stretching/shrinking sheet. Australian Journal of Mechanical Engineering. 2018;16(3):213-229.
58. Daniel YS, Zainal AA, Ismail Z, Salah F. Electrical unsteady MHD natural convection flow of nanofluid with thermal stratification and heat generation/ absorption. Matematika. 2018;34(2):393-417.
59. Daniel YS, Aziz ZA, Ismail Z, Salah F. Hydromagnetic slip flow of nanofluid with thermal stratification and convective heating. Australian Journal of Mechanical Engineering. 2018;1-9.
60. Daniel YS, Aziz ZA, Ismail Z, Salah F. Slip effects on electrical unsteady MHD natural convection flow of nanofluid over a permeable shrinking sheet with thermal radiation. Engineering Letters. 2018;26(1): 107-116.
61. Kays WM, London AL. Compact heat exchangers. 3rd. McGraw-Hill: New York, U.S.A; 1964.
62. White FM. Viscous fluid flow. McGraw-Hill: New York, U.S.A; 1974.
63. Wark K. Thermodynamics. 4th. McGraw-Hill: New York, U.S.A; 1983. Based in NASA SP-273. U. S. Government Printing Office: Washington; 1971.
64. Mioralli PC. Análise térmica de um regenerador rotativo. Master dissertation. FEM/ UNICAMP, Campinas-SP: Brazil; 2005.
65. Mioralli PC. Transferência de Calor em um Regenerador Rotativo com Perda de Carga Estabelecida nos Dutos da Matriz. Doctoral thesis. FEM/UNICAMP, Campinas-SP: Brazil; 2009. Portuguese.

© 2019 Mioralli et al.; This is an Open Access article distributed under the terms of the Creative Commons Attribution License (<http://creativecommons.org/licenses/by/4.0>), which permits unrestricted use, distribution, and reproduction in any medium, provided the original work is properly cited.

Peer-review history:
The peer review history for this paper can be accessed here:
<http://www.sdiarticle3.com/review-history/48540>